

Article

$M[B_2(SO_4)_4]$ ($M = Mn, Zn$)—Syntheses and Crystal Structures of Two New Phyllosilicate Analogue Borosulfates

Leonard C. Pasqualini ¹, Hubert Huppertz ¹  and Jörn Bruns ^{2,*} 

¹ Institute of General, Inorganic and Theoretical Chemistry, University of Innsbruck, Innrain 80-82, 6020 Innsbruck, Austria; Leonard.Pasqualini@student.uibk.ac.at (L.C.P.); Hubert.Huppertz@uibk.ac.at (H.H.)

² Institute of Inorganic Chemistry, University of Cologne, Greinstrasse 6, 50939 Cologne, Germany

* Correspondence: j.brunns@uni-koeln.de; Tel.: +49-(221)-470-76103

Received: 26 November 2019; Accepted: 10 December 2019; Published: 17 December 2019



Abstract: Borosulfates are a rapidly expanding class of silicate analogue materials, where the structural diversity is expected to be at least as large as known for silicates. However, borosulfates with cross-linking of the anionic network into two or even three dimensions are still very rare. Herein, we present two new representatives with phyllosilicate analogue topology. Through solvothermal reactions of ZnO and $MnCl_2 \cdot 4H_2O$ with boric acid in oleum (65% SO_3), we obtained single-crystals of $Mn[B_2(SO_4)_4]$ (monoclinic, $P2_1/n$, $Z = 2$, $a = 8.0435(4)$, $b = 7.9174(4)$, $c = 9.3082(4)$ Å, $\beta = 110.94(1)^\circ$, $V = 553.63(5)$ Å³) and $Zn[B_2(SO_4)_4]$ (monoclinic, $P2_1/n$, $Z = 2$, $a = 7.8338(4)$, $b = 8.0967(4)$, $c = 9.0399(4)$ Å, $\beta = 111.26(1)^\circ$, $V = 534.36(5)$ Å³). The crystal structures reveal layer-like anionic networks with alternating vierer- and zwölferringe formed exclusively by corner-linked (SO_4)- and (BO_4)-tetrahedra.

Keywords: solvothermal synthesis; crystal structure; borosulfate; manganese; zinc; X-ray diffraction

1. Introduction

The structural chemistry of silicates is dominated by anionic networks of corner-shared (SiO_4)-tetrahedra and is still a fascinating field of research for scientists from different disciplines. Friedrich Liebau is one of the pioneers in silicate chemistry and introduced a classification in 1985 [1]. According to this classification, silicates can be assigned to different classes: Nesosilicates reveal exclusively isolated (SiO_4)-tetrahedra. Isolated anionic moieties of corner-shared (SiO_4)-tetrahedra are predominant in sorosilicates. The anionic substructures of cyclosilicates contain ring-like anionic moieties of corner-shared (SiO_4)-tetrahedra with a Si:O ratio of 1:3. Inosilicates are formed by infinite anionic chains or bands. If the anionic network branches in two dimensions phyllosilicates occur, which reveal infinite anionic layers. Last but not least, silicates with 3D network like structures are called tectosilicates. The function of all previously introduced silicates is mostly related to their respective crystal structures, as well as the dimensionality of the anionic substructures [2–5].

Nowadays, several substitution variants of the aforementioned silicates are known. In these compounds, the central silicon atoms are partially or completely substituted by one or even two different atoms. Thus, the resulting anionic substructures differ by the respective atoms in the tetrahedral centers, which determine the total charge of the anionic network. Especially for aluminosilicates, alumophosphates, and borophosphates, where aluminum, phosphorous, and boron atoms reside in the center of the tetrahedra, the correlation between syntheses, structure, and properties are well explored [6–8]. Probably, the most prominent examples are microporous aluminosilicates, the so-called zeolites. Due to their open network structures, they are used as ion-conducting materials, absorbents, and catalysts [9,10].

A comparably new class of silicate analogue materials are borosulfates, with sulfur and boron occupying the position of silicon. According to Pauling's rules, networks of corner-shared tetrahedra are stable, if the respective central atoms are able to compensate the occurring charges, either by themselves or by extended crosslinking of the anionic network [11]. To branch networks with sulfur in the center of the tetrahedra into further dimensions, the high charge has to be compensated. Therefore, the combination of (SO₄)- and (BO₄)-tetrahedra [12–25] or (SO₃Cl)- and (BO₄)-tetrahedra [26–28] is suitable. The structural variety of neat borosulfates covers sorosilicate, inosilicate, phyllosilicate, and tectosilicate analogue materials. Furthermore, borosulfates can overcome Pauling's rules, which is manifested by the formation of anionic substructures with S–O–S, as well as B–O–B bridges, like in $M[B(S_2O_7)_2]$ ($M = \text{Li, Na, K, NH}_4$) [20,21,24], $M[B(SO_4)(S_2O_7)]$ ($M = \text{Cs, H}$) [21] B₂S₂O₉ [22], or $M_4[B_2O(SO_4)_6]$ ($M = \text{Mn, Co, Ni, Zn}$) [23], to mention just a few examples.

We assume that the synthesis parameters strongly influence the nature of the tetrahedral linkage. A comparison of the synthesis temperatures of literature known borosulfates gives evidence of this assumption. Accordingly, compounds with S–O–S bridges are realized at low temperatures, whereas B–O–B bridges result from synthesis at high temperatures, most likely under the release of SO₃ [20,21,23,24]. However, up to now we have no evidence for the decisive factors leading to the different dimensionalities of the anionic subunits. The most prominent representatives are 0D and 1D compounds like soro- and inosilicate analogues, if we exclude compounds with S–O–S and B–O–B bridges. 2D and 3D materials are only rarely observed. Li[B(SO₄)₂] [24] is the sole example of a borosulfate with an extended 3D network with exclusively S–O–B bridges, and phyllosilicate analogue substructures are only found for CaB₂S₄O₁₆ [18] and Mg[B₂(SO₄)₄] [25].

With this publication, we contribute two further representatives, namely Mn[B₂(SO₄)₄] and Zn[B₂(SO₄)₄], with phyllosilicate analogue substructure, charge compensated by divalent subgroup metals, obtained from solvothermal synthesis in SO₃-enriched sulfuric acid.

2. Results and Discussion

Both new borosulfates were obtained in form of colorless crystals (see Figures S1 and S2) from a solvothermal reaction with SO₃-enriched sulfuric acid in evacuated and torch sealed glass ampoules at elevated temperature (see Materials and Methods). Mn[B₂(SO₄)₄] and Zn[B₂(SO₄)₄] crystallize in the monoclinic space group $P2_1/n$ with $a = 8.0435(4)$, $b = 7.9174(4)$, $c = 9.3082(4)$ Å, $\beta = 110.94(1)^\circ$ for Mn[B₂(SO₄)₄] and $a = 7.8338(4)$, $b = 8.0967(4)$, $c = 9.0399(4)$ Å, $\beta = 111.26(1)^\circ$ for Zn[B₂(SO₄)₄] (see Table 1 and X-ray crystallography for further data and details according the refinement). The crystal structures exhibit layer-like anionic subunits of vertex-shared (BO₄)- and (SO₄)-tetrahedra (Figure 1) charge compensated by the respective divalent counter cations Mn²⁺ and Zn²⁺. Each (BO₄)-tetrahedron is coordinated by four different (SO₄)-tetrahedra via common corners, whereas for each (SO₄)-tetrahedron two oxygen atoms remain terminal. The Niggli formula for the anionic substructure of both borosulfates can be described as ${}_{\infty}^2\left\{ \left[B(SO_4)_{4/2} \right]^- \right\}$. The B–O bond lengths range from 1.440(1) to 1.485(1) Å for Mn[B₂(SO₄)₄] and from 1.449(1) to 1.482(1) Å for Zn[B₂(SO₄)₄]. With about 1.52 Å, the S–O bonds within the S–O–B bridges are significantly elongated compared to the terminal or cation coordinating S–O bonds. The latter fall in the region between 1.4125(7) to 1.4427(7) Å for Mn[B₂(SO₄)₄] and 1.4135(7) to 1.442(7) Å for Zn[B₂(SO₄)₄].

Table 1. Crystal data and structure refinement for Mn[B₂(SO₄)₄] and Zn[B₂(SO₄)₄].

Sum formula	Mn[B ₂ (SO ₄) ₄]	Zn[B ₂ (SO ₄) ₄]
Formula weight	460.80	471.23
Temperature/K	173(2)	183(2)
Crystal system	monoclinic	monoclinic
Space group	P2 ₁ /n	P2 ₁ /n
<i>a</i> /Å	8.0435(4)	7.8338(4)
<i>b</i> /Å	7.9174(4)	8.0967(4)
<i>c</i> /Å	9.3082(4)	9.0399(4)
β /°	110.94(1)	111.26(1)
Volume/Å ³	553.63(5)	534.36(5)
<i>Z</i>	2	2
ρ_{calc} /g/cm ³	2.764	2.929
μ /mm ⁻¹	2.052	3.189
<i>F</i> (000)	454	464
Crystal size/mm ³	0.07 × 0.055 × 0.03	0.5 × 0.3 × 0.11
Radiation	Mo-K α ₁ (λ = 0.71073)	Mo-K α ₁ (λ = 0.71073)
2 θ range for data collection/°	5.76 to 82.54	5.91 to 78.95
Index ranges	-14 ≤ <i>h</i> ≤ 14, -14 ≤ <i>k</i> ≤ 14, -17 ≤ <i>l</i> ≤ 17	-14 ≤ <i>h</i> ≤ 13, -14 ≤ <i>k</i> ≤ 14, -16 ≤ <i>l</i> ≤ 16
Reflections collected	58531	26941
Independent reflections	3710 [<i>R</i> _{int} = 0.0417, <i>R</i> _{sigma} = 0.0169]	3202 [<i>R</i> _{int} = 0.0278, <i>R</i> _{sigma} = 0.0151]
Data/restraints/parameters	3710/0/106	3202/0/107
Goodness-of-fit on <i>F</i> ²	1.078	1.110
Final <i>R</i> indexes [<i>I</i> ≥ 2 σ (<i>I</i> _o)]	<i>R</i> ₁ = 0.0209, <i>wR</i> ₂ = 0.0534	<i>R</i> ₁ = 0.0168, <i>wR</i> ₂ = 0.0460
Final <i>R</i> indexes [all data]	<i>R</i> ₁ = 0.0271, <i>wR</i> ₂ = 0.0553	<i>R</i> ₁ = 0.0186, <i>wR</i> ₂ = 0.0468
Largest diff. peak/hole/eÅ ⁻³	0.48/-0.61	0.64/-0.46

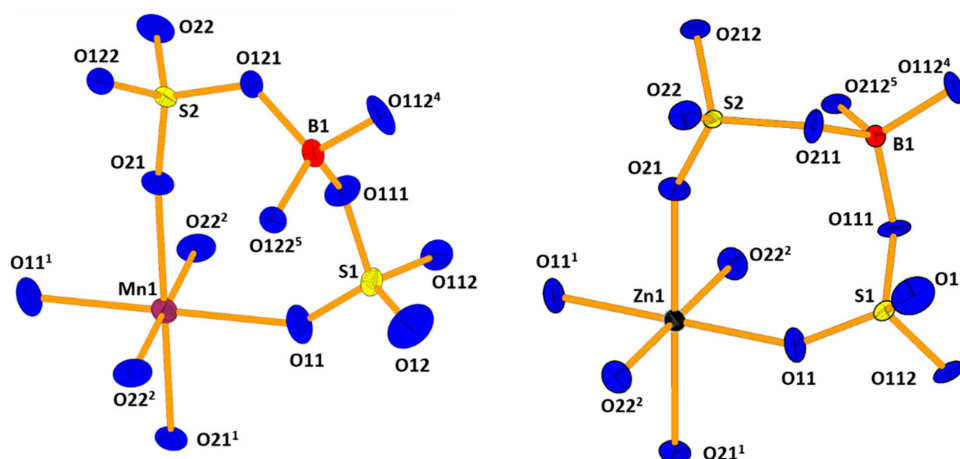


Figure 1. Left: Asymmetric unit of Mn[B₂(SO₄)₄]. The thermal ellipsoids are set on a 90% probability level. Selected bond lengths [Å]: S1–O11 1.4427(7), S1–O12 1.4125(7), S1–O111 1.5263(6), S1–O112 1.5229(6), S2–O21 1.4333(6), S2–O22 1.4298(6), S2–O212 1.5240(6), S2–O222 1.5218(6), B1–O111 1.443(1), B1–O112 1.440(1), B1–O121 1.483(1), B1–O122 1.485(1) (Symmetry operators ¹1-*x*, -*y*, 1-*z*; ²1/2+*x*, 1/2-*y*, 1/2+*z*; ³1/2-*x*, -1/2+*y*, 1/2-*z*; ⁴3/2-*x*, 1/2+*y*, 1/2-*z*; ⁵1-*x*, 1-*y*, 1-*z*); Right: Asymmetric unit of Zn[B₂(SO₄)₄]. The thermal ellipsoids are set on a 90% probability level. Selected bond lengths [Å]: S1–O11 1.4442(7), S1–O12 1.4135(7), S1–O111 1.5247(6), S1–O112 1.5315(6), S2–O21 1.4329(6), S2–O22 1.4277(6), S2–O211 1.5116(6), S2–O212 1.5116(6), B1–O111 1.458(1), B1–O112 1.449(1), B1–O211 1.477(1), B1–O212 1.482(1) (Symmetry operators ¹1-*x*, -*y*, 1-*z*; ²-1/2+*x*, 1/2-*y*, -1/2+*z*; ³3/2-*x*, -1/2+*y*, 3/2-*z*; ⁴3/2-*x*, 1/2+*y*, 1/2-*z*; ⁵1-*x*, 1-*y*, 1-*z*).

In both borosulfates, the O–S–O angles differ significantly from the perfect tetrahedral angle for both crystallographically different (SO₄)-tetrahedra. For Mn[B₂(SO₄)₄], the O–S1–O angles range from 96.18(3) to 116.59(5)°, and the O–S2–O angles range from 102.84(3) to 116.23(4)°. The comparable tetrahedra in Zn[B₂(SO₄)₄] reveal angles between 97.64(3) to 116.16(4)° for O–S1–O and 104.18(3) to 115.70(4)° for O–S2–O. The deviations are less drastic for the (BO₄)-tetrahedra. These values range from 105.67(6) to 114.05(7)° and from 101.24(6) to 114.58(6)° for Mn[B₂(SO₄)₄] and Zn[B₂(SO₄)₄], respectively

(a full list of bond lengths and angles with symmetry operators is given in the Supplementary Materials under Tables S3, S4, S7, and S8).

The layer-like anionic substructures of $\text{Mn}[\text{B}_2(\text{SO}_4)_4]$ and $\text{Zn}[\text{B}_2(\text{SO}_4)_4]$ are very similar. Both reveal twelve-membered (zwölfer) and four-membered (vierer) rings of vertex-shared (BO_4) - and (SO_4) -tetrahedra (Figure 2, top). Each zwölfer ring is surrounded by six further zwölfer rings. Two of those six are opposite to another and are aligned along the crystallographic b -axis. Each one shares two common (BO_4) -tetrahedra with the zwölfer ring. The common (BO_4) -tetrahedra are linked via two separate (SO_4) -tetrahedra, whereas each is part of one of the two zwölfer rings. As a result, a vierer ring is formed. The other four zwölfer rings share a common $(\text{BO}_4)(\text{SO}_4)(\text{BO}_4)$ -fragment and spread the network along the ac -diagonal, thereby creating a phyllosilicate analogue anionic layer. Each layer is terminated exclusively by (SO_4) -tetrahedra (Figure 2, top). However, similarities to the borophosphates also occur. With a B:P ratio <1 , compounds with condensed $[\text{B}(\text{PO}_4)_4]^{9-}$ anions occur. In this form, highly charged P^{5+} cations are located within the network as far away from each other as possible [29,30]. In the title compounds, the situation is similar. The highly charged sulfur atoms are in the center of the (SO_4) -tetrahedra, coordinated to the low charged boron cations forming repetitive $[\text{B}(\text{SO}_4)_4]$ blocks.

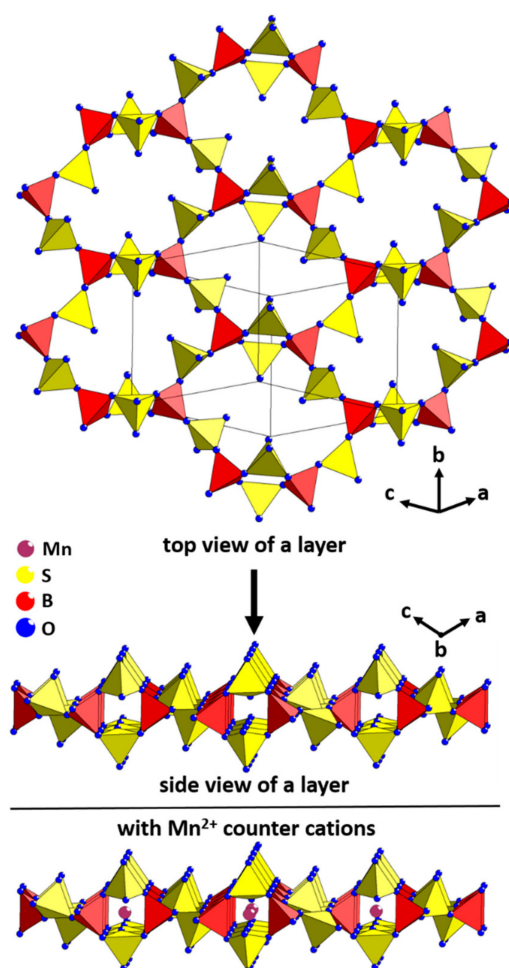


Figure 2. Top: Top view of the infinite anionic layer of vertex-shared (BO_4) - and (SO_4) -tetrahedra in the structure of $\text{Mn}[\text{B}_2(\text{SO}_4)_4]$. The layers are constructed of zwölfer and vierer rings. Each zwölfer ring is coordinated to four vierer rings and six zwölfer rings. The layers are terminated exclusively by (SO_4) -tetrahedra; **Bottom:** Side view of an infinite anionic layer. The charge compensating Mn^{2+} -cations reside within the zwölfer rings. The interspace between the different anionic layers is free of cations or intercalating molecules.

Charge compensation of the borosulfates is achieved by Mn^{2+} and Zn^{2+} cations. They are packed in a stacked manner parallel to the crystallographic b -axis in the middle of the channels running through the anionic substructures. The cations are exclusively located within the center of the zwölf rings. They are coordinated by four of their terminal oxygen atoms of (SO_4) -tetrahedra and two oxygen atoms of terminal (SO_4) -tetrahedra belonging to the anionic layers above and underneath (Figure 3). Besides $\text{B}_2\text{S}_2\text{O}_9$, a neutral vertex-shared (BO_4) - (SO_4) -network structure, only two rather similar structures are known, namely $\text{CaB}_2\text{S}_4\text{O}_{16}$ and $\text{Mg}[\text{B}_2(\text{SO}_4)_4]$. Formally, the same sum formula occurs for our new borosulfates and the known compounds. Furthermore, $\text{CaB}_2\text{S}_4\text{O}_{16}$ and $\text{Mg}[\text{B}_2(\text{SO}_4)_4]$ also exhibit zwölf and vierer rings similarly to $\text{Mn}[\text{B}_2(\text{SO}_4)_4]$ and $\text{Zn}[\text{B}_2(\text{SO}_4)_4]$. However, the positions of the cations with respect to the anionic layers are different. $\text{Mn}[\text{B}_2(\text{SO}_4)_4]$ and $\text{Zn}[\text{B}_2(\text{SO}_4)_4]$ are the first representatives with the charge compensating cations exclusively in the center of the zwölf rings. In $\text{CaB}_2\text{S}_4\text{O}_{16}$ and $\text{Mg}[\text{B}_2(\text{SO}_4)_4]$, the respective cations are located above and underneath the zwölf rings within the interlayer.

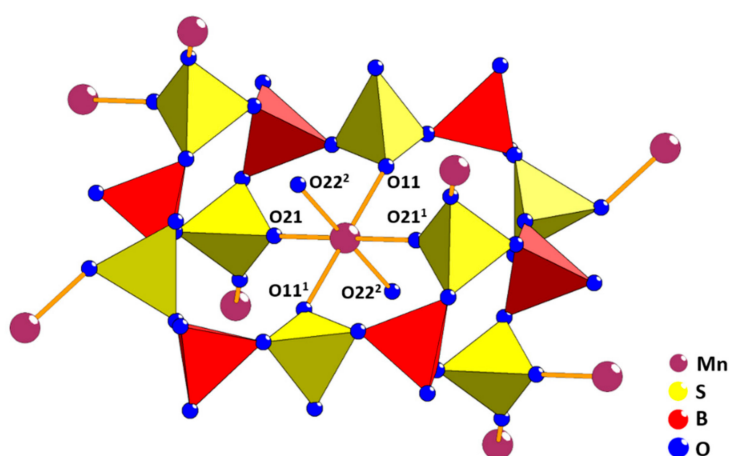


Figure 3. The Mn^{2+} cations are coordinated octahedrally by three crystallographically different oxygen atoms. Four of the six coordinating oxygen atoms belong to the terminal (SO_4) -tetrahedra of the equatorially surrounding layer, two originate from the terminal (SO_4) -tetrahedra above and underneath. Bond lengths [\AA]: Mn1-O11^1 2.1388(7), Mn1-O21^1 2.2276(6), Mn1-O22^2 2.1400(6) (Symmetry operators $^11-x,-y,1-z$; $^21/2+x,1/2-y,1/2+z$).

$\text{Mn}[\text{B}_2(\text{SO}_4)_4]$ and $\text{Zn}[\text{B}_2(\text{SO}_4)_4]$ are also not isotypical. Due to the differently rotated tetrahedra within the asymmetric unit, a structural aberration occurs between the anionic substructures of $\text{Mn}[\text{B}_2(\text{SO}_4)_4]$ and $\text{Zn}[\text{B}_2(\text{SO}_4)_4]$ (Figure 4), whereas the octahedral oxygen coordination to the metal cations remains. Focusing on one central zwölf ring in both borosulfates, the adjoining vierer rings are almost congruent. The main differences occur in the tetrahedra, forming the common $(\text{BO}_4)(\text{SO}_4)(\text{BO}_4)$ -edges to the next zwölf rings. Especially strong rotated are the (SiO_4) -tetrahedra.

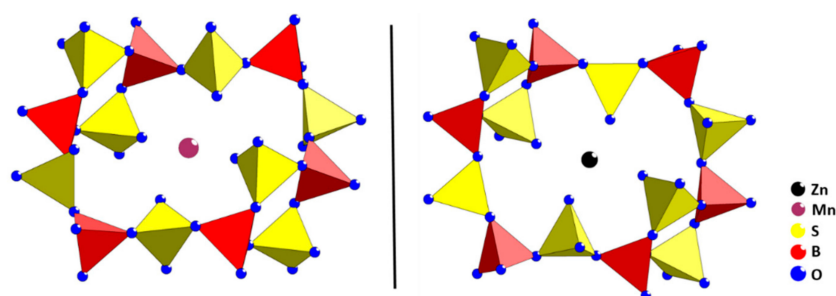


Figure 4. Differently rotated zwölf rings around Zn^{2+} and Mn^{2+} in the structures of $M[\text{B}_2(\text{SO}_4)_4]$ ($M = \text{Mn}, \text{Zn}$).

3. Materials and Methods

Synthesis of $\text{Mn}[\text{B}_2(\text{SO}_4)_4]$ and $\text{Zn}[\text{B}_2(\text{SO}_4)_4]$: $\text{MnCl}_2 \cdot 4\text{H}_2\text{O}$ (133 mg (0.67 mmol), Fluka, Seelze, Germany) or ZnO (55 mg (0.68 mmol), Merck, Darmstadt, Germany) were loaded together with H_3BO_3 (300 mg (4.85 mmol), Carl Roth, Karlsruhe, Germany), and 1 mL oleum (65% SO_3 , Merck, Darmstadt, Germany) into a thick-walled glass ampoule ($l = 300$ mm, $\varnothing = 16$ mm, thickness of the tube wall = 1.8 mm), respectively. The ampoules were torch sealed under reduced pressure (0.01 mbar), and placed into a block-shaped resistance furnace and heated up to 523 K within 150 min. The temperature was maintained for 48 h and finally reduced to 298 K within 96 h. A large number of colorless block-shaped crystals were obtained for both borosulfates (Figures S1 and S2), and the yield was quantitative for ZnO and almost quantitative for $\text{MnCl}_2 \cdot 4\text{H}_2\text{O}$. The latter suffered from small impurities of $(\text{H}_3\text{O})[\text{B}(\text{SO}_4)_2]$ (see X-ray crystallography). The crystals are very moisture sensitive and decompose immediately after exposure to air. Thus, the products were handled under strictly inert conditions.

Caution: Oleum is a strong oxidizer, which needs careful handling. During and even after the reaction, the ampoules might be under remarkable pressure. It is mandatory to cool down the ampoules using liquid nitrogen prior to opening.

X-ray crystallography: The mother liquor was separated from the crystals via decantation. The acid-containing side of the ampoule was cooled with liquid nitrogen and several crystals were transferred into inert oil directly after opening. The remaining bulk material was transferred to a glovebox for further characterization. Under a polarization microscope, a suitable crystal was prepared, mounted onto a glass needle ($\varnothing = 0.1$ mm), and immediately placed into a stream of cold N_2 (measurement temperature see Table 1) inside the diffractometer (Bruker D8 Quest κ , Bruker, Karlsruhe, Germany). After unit cell determination, the reflection intensities were collected. Structure solutions and refinements were conducted using the SHELX program package [31].

X-ray powder diffraction was carried out with a Stoe StadiP powder diffractometer (Stoe & Cie GmbH, Darmstadt, Germany) in transmission geometry on a sample washed with CCl_4 and dried under reduced pressure before the measurement. To fill a capillary with a solid sample was impossible due to small amounts of adhesive solvent. Finally, a flat sample was irradiated with Ge(111)-monochromatized $\text{Mo-K}\alpha_1$ -radiation ($\lambda = 0.7093$ Å), which was detected using a Dectris Mythen 1K detector (Dectris AG, Baden-Daettwil, Germany). Due to the fast decomposition of the sample holder matrix, the measurement had to be conducted with a scan range from 2 to 41.9° , with a step size of 2.1° and step time of 11 s. Rietveld refinement was accomplished using TOPAS4.2 [32]. Refined lattice parameters based on powder data: $\text{Mn}[\text{B}_2(\text{SO}_4)_4]$ $a = 8.082(4)$ Å, $b = 7.942(3)$ Å, $c = 9.288(8)$ Å, $\beta = 110.84(7)^\circ$, $V = 557.24(4)$ Å³; $\text{Zn}[\text{B}_2(\text{SO}_4)_4]$ $a = 7.883(5)$ Å, $b = 8.095(3)$ Å, $c = 9.034(2)$ Å, $\beta = 111.21(9)^\circ$, $V = 537.45(8)$ Å³. An amount of 11.3% $(\text{H}_3\text{O})[\text{B}(\text{SO}_4)_2]$ could be detected as a byproduct of $\text{Mn}[\text{B}_2(\text{SO}_4)_4]$ (Figure 5). Differences in the intensities of the experimental and simulated powder patterns might be due to preferred orientations of the crystalline material on the flat sample holder.

$\text{Mn}[\text{B}_2(\text{SO}_4)_4]$ and $\text{Zn}[\text{B}_2(\text{SO}_4)_4]$: The crystal structures of $\text{Mn}[\text{B}_2(\text{SO}_4)_4]$ and $\text{Zn}[\text{B}_2(\text{SO}_4)_4]$ were solved in the monoclinic space group $P2_1/n$. The heavy atom positions were determined by SHELXT-2014/5 [33] using Direct Methods. Further atoms could be successfully located by difference Fourier techniques during refinement with SHELXL-2017/1 [34]. Multi-scan absorption correction was applied to the data using the program SADABS-2014/5 by Bruker [35]. Finally, the structure and model of $\text{Mn}[\text{B}_2(\text{SO}_4)_4]$ were refined to R_1 (all data) = 0.0271 and wR_2 (all data) = 0.0553 and for $\text{Zn}[\text{B}_2(\text{SO}_4)_4]$ to R_1 (all data) = 0.0186 and wR_2 (all data) = 0.0468. Selected bond lengths and angles are presented in the Tables S3, S4, S7 and S8.

CSD 1958827 for $\text{Mn}[\text{B}_2(\text{SO}_4)_4]$ and CSD number 1958830 for $\text{Zn}[\text{B}_2(\text{SO}_4)_4]$ contain the supplementary crystallographic data for this paper. These data can be obtained free of charge from FIZ Karlsruhe via www.ccdc.cam.ac.uk/structures.

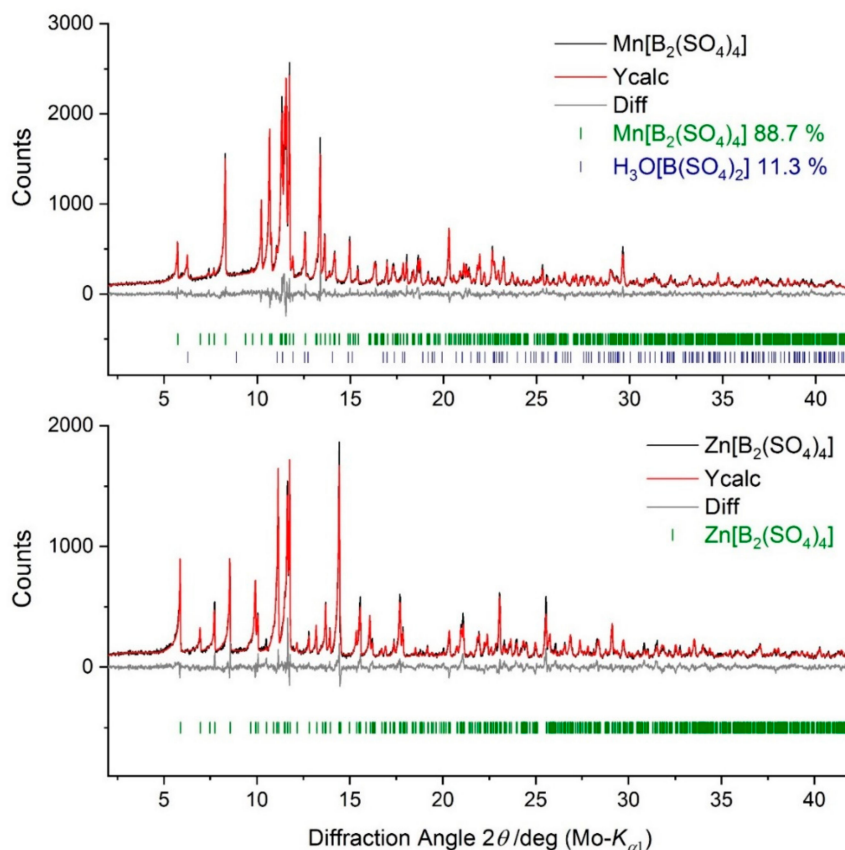


Figure 5. Rietveld refinement plot for experimental and calculated data of $M[B_2(SO_4)_4]$ ($M = Mn, Zn$). In the case of $Mn[B_2(SO_4)_4]$, about 11.3% of $(H_3O)[B(SO_4)_2]$ can be refined as a byproduct. Different intensities of experimental and calculated plots might result from the preferred orientation of the crystallites on the flat sample holder. Refined lattice parameters: $Mn[B_2(SO_4)_4]$ $a = 8.082(4) \text{ \AA}$, $b = 7.942(3) \text{ \AA}$, $c = 9.288(8) \text{ \AA}$, $\beta = 110.84(7)^\circ$, $V = 557.24(4) \text{ \AA}^3$; $Zn[B_2(SO_4)_4]$ $a = 7.883(5) \text{ \AA}$, $b = 8.095(3) \text{ \AA}$, $c = 9.034(2) \text{ \AA}$, $\beta = 111.21(9)^\circ$, $V = 537.45(8) \text{ \AA}^3$.

4. Conclusions

Reactions between oleum enriched with 65% SO_3 and boric acid in evacuated torch-sealed glass ampoules seem to be a powerful strategy to synthesize borosulfates with layer-like anionic substructures of divalent metals. As can be seen from this and our previous publications, not only the main group but also subgroup metals can be charge-compensating cations. In comparison to $Mg[B_2(SO_4)_4]$ and $CaB_2S_4O_{16}$, $Mn[B_2(SO_4)_4]$ and $Zn[B_2(SO_4)_4]$ are the first representatives of layer-like borosulfates with the cations residing in the plane of the anionic network and the center of zwoelfer rings. However, it is still unclear why cations with a comparable atomic radius like Zn^{2+} and Mg^{2+} act differently. This problem is currently under investigation using quantum chemical calculations.

Supplementary Materials: The following are available online at <http://www.mdpi.com/2304-6740/7/12/145/s1>, Figures S1 and S2: Crystals of $Zn[B_2(SO_4)_4]$ and $Mn[B_2(SO_4)_4]$ under a polarisation microscope; Table S1: Fractional atomic coordinates ($\times 10^4$) and equivalent isotropic displacement parameters ($\text{\AA}^2 \times 10^3$) for $Mn[B_2(SO_4)_4]$; Table S2: Anisotropic displacement parameters ($\text{\AA}^2 \times 10^3$) for $Mn[B_2(SO_4)_4]$; Table S3: Bond lengths for $Mn[B_2(SO_4)_4]$; Table S4: Bond angles for $Mn[B_2(SO_4)_4]$; Table S5: Fractional atomic coordinates ($\times 10^4$) and equivalent isotropic displacement parameters ($\text{\AA}^2 \times 10^3$) for $Zn[B_2(SO_4)_4]$; Table S6: Anisotropic displacement parameters ($\text{\AA}^2 \times 10^3$) for $Zn[B_2(SO_4)_4]$; Table S7: Bond lengths for $Zn[B_2(SO_4)_4]$; Table S8: Bond angles for $Zn[B_2(SO_4)_4]$; the CIF and the checkCIF output files of $Mn[B_2(SO_4)_4]$ and $Zn[B_2(SO_4)_4]$.

Author Contributions: Synthesis, preparation and characterization of the title compounds were carried out by L.C.P. under the supervision of H.H. and J.B. Supported by L.C.P., the manuscript was written by J.B. and reviewed by H.H.

Funding: L.C.P. is very grateful for the Ph.D. scholarship from the Leopold-Franzens-University Innsbruck. J.B. is thankful for the financial support of the Fonds der Chemischen Industrie (FCI).

Acknowledgments: We thank Klaus Wurst for collecting the single-crystal data and Viktoria Falkowski for the Rietveld refinement.

Conflicts of Interest: The authors declare no conflict of interest.

References

1. Liebau, F. *Structural Chemistry of Silicates*; Springer: Berlin/Heidelberg, Germany, 1985.
2. Deer, W.A.; Howie, R.A.; Zussmann, J. *An Introduction to Rock-Forming Minerals*; Langmanns: London, UK, 1966.
3. Krivovichev, S.V. *Minerals as Advanced Materials II*; Springer: Berlin/Heidelberg, Germany, 2012.
4. Ying, J.Y.; Mehnert, C.P.; Wong, M.S. Synthesis and Applications of Supramolecular-Templated Mesoporous Materials. *Angew. Chem. Int. Ed.* **1999**, *38*, 56–77. [[CrossRef](#)]
5. Wang, X.; Zhuang, J.; Chen, J.; Zhou, K.; Li, Y. Thermally Stable Silicate Nanotubes. *Angew. Chem. Int. Ed.* **2004**, *43*, 2017–2020. [[CrossRef](#)] [[PubMed](#)]
6. Oliver, S.; Kupermann, A.; Ozin, G.A. A New Model for Aluminophosphate Formation: Transformation of a Linear Chain Aluminophosphate to Chain, Layer, and Framework Structures. *Angew. Chem. Int. Ed.* **1998**, *37*, 46–62. [[CrossRef](#)]
7. Santilli, D.S.; Zones, S.I. *Synthesis of Microporous Materials: Vol. 1: Molecular Sieves*; Van Nostrand Reinhold: New York, NY, USA, 1992.
8. Kniep, R.; Gözel, G.; Eisenmann, B.; Röhr, C.; Asbrand, M.; Kizilyalli, M. Borophosphates—A Neglected Class of Compounds: Crystal Structures of $M^{II}[BPO_5]$ ($M^{II} = Ca, Sr$) and $Ba_3[BP_3O_{12}]$. *Angew. Chem. Int. Ed.* **1994**, *33*, 749–751. [[CrossRef](#)]
9. Marakatti, V.S.; Halgeri, A.B. Metal ion-exchanged Zeolites as highly active Solid acid Catalysts for the Green Synthesis of Glycerol Carbonate from Glycerol. *RSC Adv.* **2015**, *5*, 14286–14293. [[CrossRef](#)]
10. Marakatti, V.; Halgeri, A.B.; Shanbhag, G.V. Metal ion-exchanged Zeolites as Solid acid Catalysts for the Green Synthesis of nopol from Prins reaction. *Catal. Sci. Technol.* **2014**, *4*, 4065–4074. [[CrossRef](#)]
11. Pauling, L. The Principles determining the structure of complex ionic crystals. *J. Am. Chem. Soc.* **1929**, *51*, 1010–1026. [[CrossRef](#)]
12. Höpfe, H.A.; Kazmierczak, K.; Daub, M.; Förg, K.; Fuchs, F.; Hillebrecht, H. The First Borosulfate $K_5[B(SO_4)_4]$. *Angew. Chem. Int. Ed.* **2012**, *51*, 6255–6257. [[CrossRef](#)]
13. Gross, P.; Kirchhain, A.; Höpfe, H.A. The Borosulfates $K_4[BS_4O_{15}(OH)]$, $Ba[B_2S_3O_{13}]$, and $Gd_2[B_2S_6O_{24}]$. *Angew. Chem. Int. Ed.* **2016**, *55*, 4353–4355. [[CrossRef](#)]
14. Bruns, J.; Podewitz, M.; Janka, O.; Pöttgen, R.; Liedl, K.; Huppertz, H. $Cu[B_2(SO_4)_4]$ and $Cu[B(SO_4)_2(HSO_4)]$ —Two silicate analogue borosulfates differing in their dimensionality: A comparative study of stability and acidity. *Angew. Chem. Int. Ed.* **2018**, *130*, 9693–9697. [[CrossRef](#)]
15. Netzsch, P.; Hämmer, M.; Gross, P.; Bariss, H.; Block, T.; Heletta, L.; Pöttgen, R.; Bruns, J.; Huppertz, H.; Höpfe, H.A. $RE_2[B_2(SO_4)_6]$ ($RE = Y, La-Nd, Sm, Eu, Tb-Lu$): A silicate-analogues host structure with weak coordination behaviour. *Dalton Trans.* **2019**, *48*, 4387–4397. [[CrossRef](#)]
16. Bruns, J.; Podewitz, M.; Schauperl, M.; Liedl, K.; Janka, O.; Pöttgen, R.; Huppertz, H. $Ag[B(SO_4)_2]$ —Synthesis, crystal structure and characterization of the first precious-metal borosulfate. *Eur. J. Inorg. Chem.* **2017**, *34*, 3981–3989. [[CrossRef](#)]
17. Schönegger, S.; Bruns, J.; Gartner, B.; Wurst, K.; Liedl, K.; Huppertz, H. Synthesis and characterization of the first lead(II) borosulfate $Pb[B_2(SO_4)_4]$. *Z. Allg. Anorg. Chem.* **2018**, *644*, 1702–1706. [[CrossRef](#)]
18. Bruns, J.; Podewitz, M.; Schauperl, M.; Joachim, B.; Liedl, K.; Huppertz, H. $CaB_2S_4O_{16}$: A borosulfate exhibiting a new structure type with phyllosilicate topology. *Chem. Eur. J.* **2017**, *23*, 16773–16781. [[CrossRef](#)]
19. Daub, M.; Hillebrecht, H. Borosulfates $Cs_2B_2S_3O_{13}$, $Rb_4B_2S_4O_{17}$, and $A_3HB_4S_2O_{14}$ ($A = Rb, Cs$)—Crystalline Approximants for Vitreous B_2O_3 ? *Eur. J. Inorg. Chem.* **2015**, *2015*, 4176–4181. [[CrossRef](#)]
20. Daub, M.; Höpfe, H.A.; Hillebrecht, H. Further New Borosulfates: Synthesis, crystal Structure, and vibrational spectra of $A[B(SO_4)_2]$ ($A = Na, K, NH_4$) and the crystal structures of $Li_5[B(SO_4)_4]$ and $NH_4[B(S_2O_7)_2]$. *Z. Anorg. Allg. Chem.* **2014**, *640*, 2914–2921. [[CrossRef](#)]

21. Daub, M.; Kazmierczak, K.; Höpfe, H.A.; Hillebrecht, H. The borosulfate story goes on—From alkali and oxonium salts to polyacids. *Chem. Eur. J.* **2013**, *19*, 16954–16962. [[CrossRef](#)] [[PubMed](#)]
22. Logemann, C.; Wickleder, M.S. B₂S₂O₉—A boron sulfate with phyllosilicate topology. *Angew. Chem. Int. Ed.* **2013**, *52*, 14229–14232. [[CrossRef](#)]
23. Netzsch, P.; Gross, P.; Takahashi, H.; Höpfe, H.A. Synthesis and characterization of the first borosulfates of magnesium, manganese, cobalt nickel, and zinc. *Inorg. Chem.* **2018**, *57*, 8530–8539. [[CrossRef](#)]
24. Daub, M.; Kazmierczak, K.; Gross, P.; Höpfe, H.A.; Hillebrecht, H. Exploring a New Structure Family: Alkali Borosulfates Na₅[B(SO₄)₄], A₃[B(SO₄)₃] (A = K, Rb), Li[B(SO₄)₂], and Li[B(S₂O₇)₂]. *Inorg. Chem.* **2013**, *52*, 6011–6020. [[CrossRef](#)]
25. CSD-434487. Available online: www.ccdc.cam.ac.uk/structures (accessed on 11 December 2019).
26. Mairesse, G.; Drache, M. The Crystal Structure of Potassium Tetraehlorosulfatoborate, K[B(SO₃Cl)₄]. *Acta Cryst.* **1978**, *34*, 1771–1776. [[CrossRef](#)]
27. Marsch, R.E. Potassium tetrachlorosulfatoborate: Change in space group. *Acta Cryst.* **1980**, *36*, 219–220. [[CrossRef](#)]
28. Mairesse, G.; Drache, M. Lithium Tetrakis(chlorosulfato)borate. *Acta Cryst.* **1980**, *36*, 2767–2768. [[CrossRef](#)]
29. Ruchkina, E.A.; Belokoneva, E.L. Structural Features of Pb, Fe, and Alkali Metal Borophosphates as analysed in terms of topologically similar structural blocks. *Russ. J. Inorg. Chem.* **2003**, *48*, 1812–1821.
30. Kniep, R.; Schäfer, G.; Engelhardt, G.; Boy, I. K[ZnBP₂O₈] and A[ZnBP₂O₈] (A = NH₄⁺, Rb⁺, Cs⁺): Zincoborophosphates as a New Class of Compounds with Tetrahedral Framework Structures. *Angew. Chem. Int. Ed.* **1999**, *38*, 3642–3644. [[CrossRef](#)]
31. Sheldrick, G.M. A short history of *SHELX*. *Acta Cryst.* **2008**, *64*, 112–122. [[CrossRef](#)]
32. *TOPAS4.2*; Bruker: Karlsruhe, Germany, 2009.
33. Sheldrick, G.M. *SHELXT*—Integrated space-group and crystal-structure determination. *Acta Cryst. Sect. A* **2015**, *71*, 3–8. [[CrossRef](#)]
34. Sheldrick, G.M. Crystal structure refinement with *SHELXL*. *Acta Cryst. Sect. C* **2015**, *71*, 3–8. [[CrossRef](#)]
35. Sheldrick, G.M. *SADABS 2014/5*; University of Göttingen: Göttingen, Germany, 1996.



© 2019 by the authors. Licensee MDPI, Basel, Switzerland. This article is an open access article distributed under the terms and conditions of the Creative Commons Attribution (CC BY) license (<http://creativecommons.org/licenses/by/4.0/>).